JOURNAL OF AIRCRAFT
Vol. 41, No. 6, November–December 2004

Order Reduction of State-Space Aeroelastic Models Using Optimal Modal Analysis

Taehyoun Kim,* Kanivenahalli S. Nagaraja,† and Kumar G. Bhatia‡
Boeing Commercial Aircraft, Seattle, Washington 98124-2207

An efficient time-domain reduced-order aeroelastic model is presented based on the Roger's state-space rational function approximation model and the frequency-domain Karhunen–Loeve method. Using frequency responses of the Roger's model, the method generates a real, orthogonal set of aeroelastic modes. These Karhunen–Loeve modes are optimal in the solution space with a minimum possible number of modes. When invoked with the Galerkin's error minimization, they generate a reduced-order aeroelastic model. The proposed method is demonstrated using an aeroelastic model of a representative commercial airplane with 638 state variables. It is shown that the aeroelastic results of the reduced-order model match extremely well the results obtained from the full-order model in both open-loop and closed-loop analyses. The new aeroelastic model can be efficiently used in repeated analysis of dynamic loads, optimization, and closed-loop designs.

Nomenclature

$\boldsymbol{AB}_g\boldsymbol{B}_\delta$	=	aeroelastic system matrices
$\boldsymbol{A}_c\boldsymbol{B}_c\boldsymbol{C}_c$	=	feedback system matrices
$\boldsymbol{A}_0\boldsymbol{A}_1\boldsymbol{A}_2$	=	aerodynamic system matrices in Eq. (2)
b	=	reference length
$\boldsymbol{C}$	=	generalized damping matrix
$\boldsymbol{C}_y\boldsymbol{D}_g\boldsymbol{D}_\delta$	=	aeroelastic output matrices
$\boldsymbol{C}_z\boldsymbol{D}_{zg}\boldsymbol{D}_{z\delta}$	=	measurement matrices
$\boldsymbol{DER}$	=	aerodynamic system matrices in Eq. (2)
$\boldsymbol{F}$	=	snapshot matrix as defined in Eq. (20)
$\boldsymbol{G}_g$	=	loop transfer function caused by gust input
$\boldsymbol{G}_\delta$	=	loop transfer function caused by command input
$\boldsymbol{H}_g$	=	compensator transfer function caused by gust input
$\boldsymbol{H}_x$	=	compensator transfer function caused by states
j	=	$\equiv\sqrt{-1}$
$\boldsymbol{K}$	=	generalized stiffness matrix
$\boldsymbol{K}_{\text{cs}}$	=	control command matrix
k	=	reduced frequency ($\equiv \omega b/V$)
L	=	dimension of state vector $\boldsymbol{x}$
M	=	number of frequency samples
$\boldsymbol{M}$	=	generalized mass matrix
N	=	number of generalized structural modes
$\boldsymbol{p}$	=	$(R \times 1)$ generalized coordinate vector
$\boldsymbol{Q}$	=	generalized aerodynamic force matrix for structural modes
$\boldsymbol{Q}_g$	=	generalized aerodynamic force matrix for gust
$\boldsymbol{q}$	=	$(N \times 1)$ generalized structural coordinate vector
q_d	=	dynamic pressure ($\equiv \frac{1}{2}\rho V^2$)
R	=	number of selected Karhunen-Loeve modes
$\bar{s}$	=	reduced Laplace variable ($\equiv sb/V$)
t	=	real time
$\boldsymbol{u}_g$	=	gust input vector
$\boldsymbol{\mathcal{U}}_g$	=	frequency response of $\boldsymbol{u}_g$
V	=	freestream air speed
$\boldsymbol{x}$	=	$(L \times 1)$ aeroelastic state vector
$\boldsymbol{\mathcal{X}}$	=	frequency response of $\boldsymbol{x}$
$\boldsymbol{y}$	=	output state vector
$\boldsymbol{y}_c$	=	measurement vector
$\boldsymbol{z}_c$	=	feedback control state vector
$\boldsymbol{z}_g$	=	aerodynamic lag state vector
$\boldsymbol{\alpha}$	=	eigenvector of Eq. (19)
α_g	=	gust input
$\boldsymbol{\alpha}_g$	=	frequency response of α_g
δ_c	=	control command input
$\boldsymbol{\delta}_c$	=	frequency response of δ_c
$\bar{\lambda}$	=	eigenvalue of Eq. (19)
τ	=	reduced time ($\equiv Vt/b$)
$\boldsymbol{\Phi}$	=	$(L \times R)$ KL modal matrix
ϕ	=	KL mode
Ω	=	maximum sampling frequency, rad/s
ω	=	frequency, rad/s

Presented as Paper AIAA-2001-1524 at the AIAA/ASME/ASCE/AHS/ASC 42nd SDM Conference, Seattle, WA, 16 April 2001; received 20 September 2001; revision received 22 January 2004; accepted for publication 22 January 2004.

*Principal Engineer, MS 03-KR; taehyoun.kim@pss.boeing.com. Member AIAA.
†Associate Technical Fellow.
‡Senior Technical Fellow. Associate Fellow AIAA.

Introduction

In the past, several techniques were developed for reduced-order unsteady aeroelastic modeling in the time domain. These methods include rational function approximation (RFA),[1–4] p-transformation,[5,6] and eigenformulation.[7] In particular, the RFA methods that transform complex aerodynamic forces into the time domain by rational approximation of the unsteady aerodynamic forces have been extensively used in conjunction with the doublet-lattice method.

By far the most favored reduced-order aeroelastic model is based upon Roger's RFA method.[1] Although it is well known for its accuracy and convenience of model construction, the Roger's model has often been criticized for introducing too many aerodynamic lag states. These auxiliary states are necessary to account for unsteady aerodynamic lag effects associated with structural modes accurately. Because the number of the lag states is proportional to the number of structural modes, the method becomes computationally less efficient when a large number of structural modes are used to describe complex aeroelastic behavior. The minimum-state RFA method[2,3] reduces the number of the lag states by employing a single set of lag terms and incorporating physical weights for different aerodynamic terms, but can introduce inaccuracy during the minimization. On the other hand, the p-transformation[5,6] finds complex aeroelastic eigenvectors based on the classical p-k method and performs a coordinate transformation to build a state-space aeroelastic model. Because the p-k iterations are required only for the structural states, the size of the p-transform model is precisely twice the number of the structural degrees of freedom.

In this paper, the frequency-domain Karhunen–Loeve (FDKL) method developed by Kim[8] is applied to reduce the size of the Roger's RFA aeroelastic model. Based on a finite number of frequency-response samples of the full model, the FDKL procedure seeks optimal aeroelastic modes that would span the solution space with a minimum possible number of the modes. The general response of the system is then expressed in terms of a few KL modes. When the Galerkin's error minimization is applied, these modes generate a reduced-order aeroelastic model in state-space form. To demonstrate the efficiency and accuracy of the proposed reduction scheme, an aeroelastic model of a representative commercial airplane with 638 state variables is studied. For optimal mode calculation, an elevator control surface command as well as a vertical gust in the form of impulse input are used to generate open-loop frequency responses. The resulting reduced-order model can accurately predict open-loop responses caused by combinations of any types of the gust and control inputs and closed-loop responses to the gust. Aeroelastic results of the reduced-order model both in the time and frequency domains are presented and compared with results obtained from the full-order model.

Full-Order Aeroelastic Model

For frequency-based unsteady aerodynamic models (e.g., doublet-lattice), one needs a conversion to the time domain for transient analyses. The general form of aeroelastic equation with frequency-domain aerodynamic loads is

$$\boldsymbol{M}\ddot{\boldsymbol{q}} + \boldsymbol{C}\dot{\boldsymbol{q}} + \boldsymbol{K}\boldsymbol{q} - q_d\boldsymbol{Q}\boldsymbol{q} = q_d\boldsymbol{Q}_g\alpha_g + \boldsymbol{K}_{\mathrm{cs}}\delta_c \tag{1}$$

where $\boldsymbol{q}$ represents generalized structural coordinates associated with structural modes. Given N modes, $\boldsymbol{q}$ is $(N \times 1)$ vector. Based on the Roger's original method, the generalized unsteady aerodynamic loads can be approximated in the following rational function form, which is also known as the minimum state formulation[2]:

$$\boldsymbol{Q} \simeq \boldsymbol{A}_0 + \boldsymbol{A}_1\,\bar{s} + \boldsymbol{A}_2\,\bar{s}^2 + \boldsymbol{D}(\bar{s}\,\boldsymbol{I} - \boldsymbol{R})^{-1}\boldsymbol{E}\,\bar{s} \tag{2}$$

and similarly for the gust aerodynamic force $\boldsymbol{Q}_g$:

$$\boldsymbol{Q}_g \simeq \boldsymbol{A}_{g\,0} + \boldsymbol{A}_{g\,1}\,\bar{s} + \boldsymbol{D}_g(\bar{s}\,\boldsymbol{I} - \boldsymbol{R}_g)^{-1}\boldsymbol{E}_g\,\bar{s} \tag{3}$$

Open-Loop System

Inserting the state-space aerodynamic approximations of Eqs. (2) and (3) into Eq. (1) results in the following open-loop aeroelastic equation:

$$\begin{Bmatrix} \dot{\boldsymbol{q}} \\ \ddot{\boldsymbol{q}} \\ \dot{\boldsymbol{z}} \\ \dot{\boldsymbol{z}}_g \end{Bmatrix} = \begin{bmatrix} 0 & \boldsymbol{I} & 0 & 0 \\ -\bar{\boldsymbol{M}}^{-1}\bar{\boldsymbol{K}} & -\bar{\boldsymbol{M}}^{-1}\bar{\boldsymbol{C}} & q_d\bar{\boldsymbol{M}}^{-1}\boldsymbol{D} & q_d\bar{\boldsymbol{M}}^{-1}\boldsymbol{D}_g \\ 0 & \boldsymbol{E} & \left(\dfrac{V}{b}\right)\boldsymbol{R} & 0 \\ 0 & 0 & 0 & \left(\dfrac{V}{b}\right)\boldsymbol{R}_g \end{bmatrix} \times \begin{Bmatrix} \boldsymbol{q} \\ \dot{\boldsymbol{q}} \\ \boldsymbol{z} \\ \boldsymbol{z}_g \end{Bmatrix} + \begin{bmatrix} 0 & 0 \\ q_d\bar{\boldsymbol{M}}^{-1}\boldsymbol{A}_{g0} & q_d\left(\dfrac{b}{V}\right)\bar{\boldsymbol{M}}^{-1}\boldsymbol{A}_{g1} \\ 0 & 0 \\ 0 & \boldsymbol{E}_g \end{bmatrix} \times \begin{Bmatrix} \boldsymbol{\alpha}_g \\ \dot{\boldsymbol{\alpha}}_g \end{Bmatrix} + \begin{bmatrix} 0 \\ \bar{\boldsymbol{M}}^{-1}\boldsymbol{K}_{\mathrm{cs}} \\ 0 \\ 0 \end{bmatrix} \delta_c \tag{4}$$

where

$$\bar{\boldsymbol{M}} \equiv \boldsymbol{M} - q_d\,(b/V)^2\,\boldsymbol{A}_2 \tag{5}$$

$$\bar{\boldsymbol{C}} \equiv \boldsymbol{C} - q_d\,(b/V)\,\boldsymbol{A}_1 \tag{6}$$

$$\bar{\boldsymbol{K}} \equiv \boldsymbol{K} - q_d\,\boldsymbol{A}_0 \tag{7}$$

Denoting $\boldsymbol{x} \equiv \lfloor \boldsymbol{q}\,\dot{\boldsymbol{q}}\,\boldsymbol{z}\,\boldsymbol{z}_g \rfloor^T$, $\boldsymbol{u}_g \equiv \lfloor \alpha_g\,\dot{\alpha}_g \rfloor^T$, one can write Eq. (4) in an abbreviated form as

$$\dot{\boldsymbol{x}} = \boldsymbol{A}\,\boldsymbol{x} + \boldsymbol{B}_g\,\boldsymbol{u}_g + \boldsymbol{B}_\delta\,\delta_c \qquad (L \times 1) \tag{8}$$

Once the state variables are calculated, outputs such as displacements or loads can be obtained by

$$\boldsymbol{y} = \boldsymbol{C}_y\boldsymbol{x} + \boldsymbol{D}_g\,\boldsymbol{u}_g + \boldsymbol{D}_\delta\delta_c \tag{9}$$

Equations (8) and (9) define the RFA aeroelastic model.

Closed-Loop System

For closed-loop modeling, a feedback system based on output measurements is constructed as follows:

$$\dot{\boldsymbol{z}}_c = \boldsymbol{A}_c\boldsymbol{z}_c + \boldsymbol{B}_c\boldsymbol{y}_c \tag{10}$$

$$\delta_c = \boldsymbol{C}_c\boldsymbol{z}_c \tag{11}$$

The measured signals are related to the system state via

$$\boldsymbol{y}_c = \boldsymbol{C}_z\boldsymbol{x} + \boldsymbol{D}_{z\mathrm{g}}\boldsymbol{u}_g + \boldsymbol{D}_{z\delta}\delta_c \tag{12}$$

Hence, inserting Eq. (12) into Eq. (10) and combining the equation with Eq. (8) yields the following state-space model of the closed-loop system:

$$\begin{Bmatrix} \dot{\boldsymbol{x}} \\ \dot{\boldsymbol{z}}_c \end{Bmatrix} = \begin{bmatrix} \boldsymbol{A} & \boldsymbol{B}_\delta\boldsymbol{C}_c \\ \boldsymbol{B}_c\boldsymbol{C}_z & \boldsymbol{A}_c + \boldsymbol{B}_c\boldsymbol{D}_{z\delta}\boldsymbol{C}_c \end{bmatrix} \begin{Bmatrix} \boldsymbol{x} \\ \boldsymbol{z}_c \end{Bmatrix} + \begin{bmatrix} \boldsymbol{B}_g \\ \boldsymbol{B}_c\boldsymbol{D}_{z\mathrm{g}} \end{bmatrix} \boldsymbol{u}_g \tag{13}$$

Output states of the closed-loop model can be obtained via

$$\boldsymbol{y} = [\boldsymbol{C}_y \quad \boldsymbol{D}_\delta\boldsymbol{C}_c] \begin{Bmatrix} \boldsymbol{x} \\ \boldsymbol{z}_c \end{Bmatrix} + \boldsymbol{D}_g\boldsymbol{u}_g \tag{14}$$

Note that the closed-loop Eq. (13) has been augmented by the number of control states in $\boldsymbol{z}_c$.

Frequency-Domain Karhunen–Loeve Method

The FDKL procedure[8] seeks a set of optimal modes of a dynamic system denoted as ϕ, given a frequency response of the open-loop system $\mathcal{X}(\omega)$. This is done by maximizing an energy represented by an inner product between the response and the mode in the frequency domain,

$$J(\phi) \equiv \int_{-\Omega}^{\Omega} (\phi, \mathcal{X})^2\,\mathrm{d}\omega \tag{15}$$

with the constraint

$$h(\phi) \equiv (\phi, \phi) - \int_{-\Omega}^{\Omega} (\mathcal{X}, \mathcal{X})^2\,\mathrm{d}\omega = 0 \tag{16}$$

where Ω is the maximum frequency of interest. In the case of finite dimensional space, the inner product $(,)$ is interpreted as a vector product between two vectors. Hence, one can rewrite Eqs. (15) and (16) as

$$J \equiv \int_{-\Omega}^{\Omega} |\phi^T\mathcal{X}|^2\,\mathrm{d}\omega \tag{17}$$

$$h(\phi) \equiv \|\phi\|_2^2 - \int_{-\Omega}^{\Omega} \|\mathcal{X}\|_2^2\,\mathrm{d}\omega = 0 \tag{18}$$

where $\| \ \|_2$ denotes the L_2 norm. By approximating the integral in Eq. (15) with a finite number of samples, $\mathcal{X}^{(1)}, \mathcal{X}^{(2)}, \ldots, \mathcal{X}^{(M)}$ at M sample points $\omega_1, \omega_2, \ldots, \omega_M (\omega_1 \equiv -\Omega, \omega_M \equiv \Omega)$, and assuming that the modes are linear combinations of the frequency responses, the so-called snapshot method can be formulated:

$$\boldsymbol{\Delta\omega}^{\frac{1}{2}} \boldsymbol{F} \boldsymbol{\Delta\omega}^{\frac{1}{2}} \boldsymbol{\alpha}_i = \bar{\lambda}_i \boldsymbol{\alpha}_i \qquad (i = 1, 2, \ldots, M) \tag{19}$$

where

$$F_{ij} \equiv \mathcal{X}^{(i)*T} \mathcal{X}^{(j)} \qquad (M \times M) \tag{20}$$

$$\boldsymbol{\Delta\omega}^{\frac{1}{2}} \equiv \operatorname{diag}\left(\sqrt{\Delta\omega_i}\right) \qquad (M \times M) \tag{21}$$

and $\Delta\omega_i$ represents a step size at the ith sample point. After the eigenvectors of Eq. (19) are found, the optimal modes are obtained via

$$\phi_i \equiv \left[\mathcal{X}^{(1)} \mathcal{X}^{(2)} \ldots \mathcal{X}^{(M)}\right] \boldsymbol{\Delta\omega}^{\frac{1}{2}} \boldsymbol{\alpha}_i \qquad (i = 1, 2, \ldots, M) \tag{22}$$

It can be shown that ϕ_i are real and orthonormal.[8] Furthermore, they are optimal in that they span the solution space with the minimum possible error over the class of all admissible basis sets.[9,10] The system response can be approximated as a linear combination of a few modes as

$$\boldsymbol{x}(t) \simeq \sum_{i=1}^{R} p_i(t) \phi_i \qquad (R \leq M) \tag{23}$$

It can be also shown that $\bar{\lambda}_i = J(\phi_i)$. That is, $\bar{\lambda}_i$ represents how much ϕ_i participates in the energy defined by Eq. (15). Therefore, one can select the modes in Eq. (23) such that they correspond to the largest first R eigenvalues in descending order of magnitude. For best approximation, one needs to take all of the linearly independent modes, the number of which would be equal to the rank of the covariance matrix in Eq. (19).

If the aeroelastic model of Eq. (8) is subjected to more than one input simultaneously, it might be necessary to perform the KL procedure multiple times producing multiple sets of modes. The modes obtained herein will be optimal within each set, but not so between different sets. As an alternative, given N_u number of inputs one might consider maximizing the following energy[11]:

$$J_m(\phi) \equiv \sum_{i=1}^{N_u} W_i \int_{-\Omega}^{\Omega} \left|\phi^T \mathcal{X}_i\right|^2 \mathrm{d}\omega \tag{24}$$

with the new constraint

$$h_m(\phi) \equiv \|\phi\|_2^2 - \sum_{i=1}^{N_u} W_i \int_{-\Omega}^{\Omega} \|\mathcal{X}_i\|_2^2 \, \mathrm{d}\omega = 0 \tag{25}$$

where $\mathcal{X}_i$ is the response to the ith input and W_i are scalar weights that put relative importances on the inputs.

Choice of Frequency Samples for Optimal Mode Calculation

As pointed out in Ref. 8, the KL method is a noncausal procedure in that the modes cannot be obtained unless a system response is known a priori. For this reason, it is crucial to sample a response that is most representative of the dynamic problem under consideration. Our major goal is to obtain optimal modes ϕ_i that can span as broad a range of responses $\boldsymbol{x}(t)$ as possible. For this purpose, it is helpful to examine the state response in terms of two loop transfer functions:

Open-loop:

$$\boldsymbol{\mathcal{X}}_{\mathrm{OL}}(\omega) = \boldsymbol{G}_g \boldsymbol{\mathcal{U}}_g + \boldsymbol{G}_\delta \boldsymbol{\delta}_c \tag{26}$$

Closed-loop:

$$\boldsymbol{\mathcal{X}}_{\mathrm{CL}}(\omega) = (\boldsymbol{I} + \boldsymbol{G}_\delta \boldsymbol{H}_x)^{-1} (\boldsymbol{G}_g - \boldsymbol{G}_\delta \boldsymbol{H}_g) \boldsymbol{\mathcal{U}}_g \tag{27}$$

where

$$\boldsymbol{G}_g(\omega) \equiv (j\omega \boldsymbol{I} - \boldsymbol{A})^{-1} \boldsymbol{B}_g \tag{28}$$

$$\boldsymbol{G}_\delta(\omega) \equiv (j\omega \boldsymbol{I} - \boldsymbol{A})^{-1} \boldsymbol{B}_\delta \tag{29}$$

$$\boldsymbol{H}_x(\omega) \equiv -\boldsymbol{C}_c (j\omega \boldsymbol{I}_c - \boldsymbol{A}_c - \boldsymbol{B}_c \boldsymbol{D}_{z\delta} \boldsymbol{C}_c)^{-1} \boldsymbol{B}_c \boldsymbol{C}_z \tag{30}$$

$$\boldsymbol{H}_g(\omega) \equiv -\boldsymbol{C}_c (j\omega \boldsymbol{I}_c - \boldsymbol{A}_c - \boldsymbol{B}_c \boldsymbol{D}_{z\delta} \boldsymbol{C}_c)^{-1} \boldsymbol{B}_c \boldsymbol{D}_{\mathrm{zg}} \tag{31}$$

From Eq. (26), given an input $\boldsymbol{\mathcal{U}}_g(\omega)$ or $\boldsymbol{\delta}_c(\omega)$ getting the loop transfer function $\boldsymbol{G}_g(\omega)$ or $\boldsymbol{G}_\delta(\omega)$ will guarantee a correct open-loop response caused by either type of input. On the other hand, Eq. (27) indicates that both loop transfer functions must be accounted for in the mode calculation to ensure the correct closed-loop response. For the purpose of taking snapshots, a unit impulse input is used, that is, $\boldsymbol{\alpha}_g(\omega) = \boldsymbol{\delta}_c(\omega) = 1$, and the corresponding open-loop frequency responses are sampled at the discrete sampling points.

Reduced-Order Aeroelastic Model

Inserting Eq. (23) into Eq. (8) produces a nonzero residual vector as

$$\varepsilon \equiv \boldsymbol{\Phi}\dot{\boldsymbol{p}} - \boldsymbol{A}\boldsymbol{\Phi}\boldsymbol{p} - \boldsymbol{B}_g \boldsymbol{u}_g - \boldsymbol{B}_\delta \delta_c \neq 0 \tag{32}$$

where $\boldsymbol{\Phi} \equiv [\phi_1 \phi_2 \ldots \phi_R]$. According to the Galerkin's approximation, one minimizes the error by requiring the residual be orthogonal to the basis vectors as

$$(\phi_i, \varepsilon) = 0 \qquad (i = 1, 2, \ldots, R) \tag{33}$$

This leads to the following reduced set of aeroelastic equations:

$$\dot{\boldsymbol{p}} = \boldsymbol{A}_R \boldsymbol{p} + \boldsymbol{B}_{\mathrm{gR}} \boldsymbol{u}_g + \boldsymbol{B}_{\delta R} \delta_c \qquad (R \times 1) \tag{34}$$

where

$$\boldsymbol{A}_R \equiv \boldsymbol{\Phi}^T \boldsymbol{A} \boldsymbol{\Phi} \tag{35}$$

$$\boldsymbol{B}_{gR} \equiv \boldsymbol{\Phi}^T \boldsymbol{B}_g \tag{36}$$

$$\boldsymbol{B}_{\delta R} \equiv \boldsymbol{\Phi}^T \boldsymbol{B}_\delta \tag{37}$$

Likewise, the output equation (9) is modified as

$$\boldsymbol{y} = \boldsymbol{C}_{\mathrm{yR}} \boldsymbol{p} + \boldsymbol{D}_g \boldsymbol{u}_g + \boldsymbol{D}_\delta \delta_c \tag{38}$$

where $\boldsymbol{C}_{yR} \equiv \boldsymbol{C}_y \boldsymbol{\Phi}$. Equations (34) and (38) now define the reduced-order aeroelastic model.

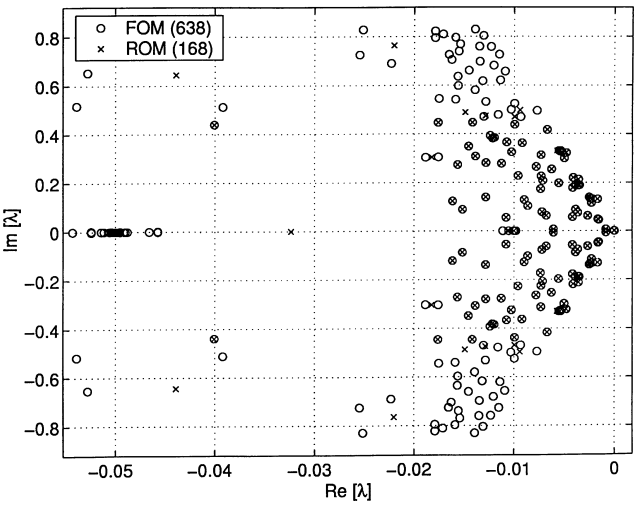

Fig. 1 Aeroelastic root loci of a commercial aircraft (open loop).

A reduced-order closed-loop model can be obtained by combining Eq. (34) with the feedback system Eqs. (10–12):

$$\begin{Bmatrix} \dot{p} \\ \dot{z}_c \end{Bmatrix} = \begin{bmatrix} A_R & B_{\delta R} C_c \\ B_c C_z \Phi & A_c + B_c D_{z\delta} C_c \end{bmatrix} \begin{Bmatrix} p \\ z_c \end{Bmatrix} + \begin{bmatrix} B_{\mathrm{gR}} \\ B_c D_{\mathrm{zg}} \end{bmatrix} u_g \quad (39)$$

For output calculation,

$$y = [C_{\mathrm{yR}} \quad D_\delta C_c] \begin{Bmatrix} p \\ z_c \end{Bmatrix} + D_g u_g \quad (40)$$

Results and Discussion

The proposed optimal model reduction method was applied to a state-space aeroelastic model of a representative commercial airplane. The structural model had been obtained from ELFINI[12] Finite Element program and has 101 symmetric and antisymmetric structural modes including six rigid-body modes and one for elevator control surface. The generalized aerodynamic forces for these modes were generated by the doublet-lattice method at 10 reduced frequencies in the range of (0, 1). The generalized aerodynamic forces for vertical gust were also generated within the same range at 17 reduced frequencies at four different gust penetration zones. The frequency-based aerodynamic forces were converted to the time

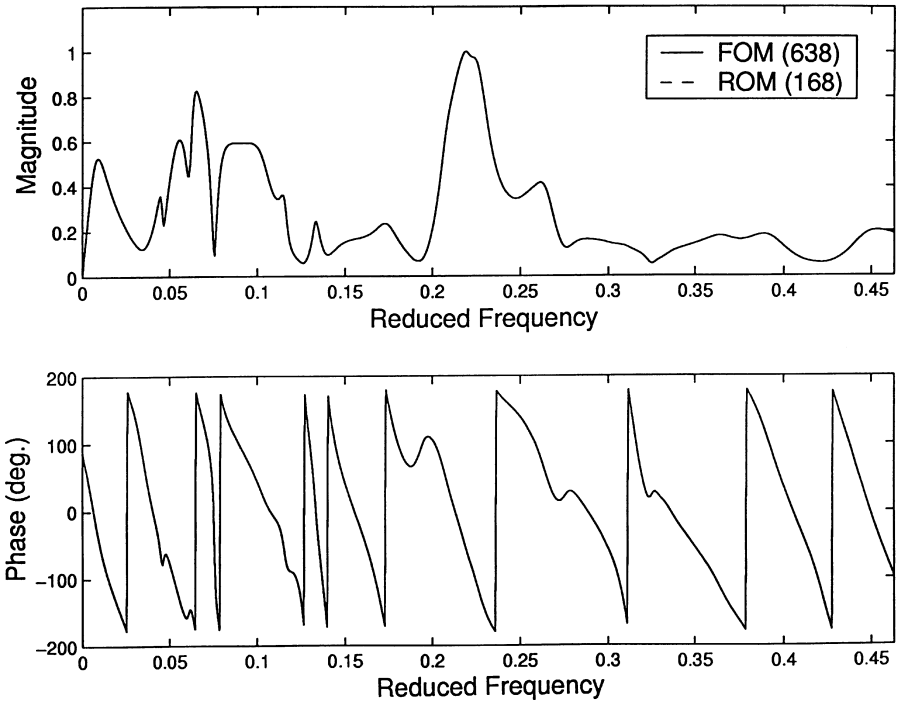

Fig. 2 Pitch rate caused by unit gust (open loop).

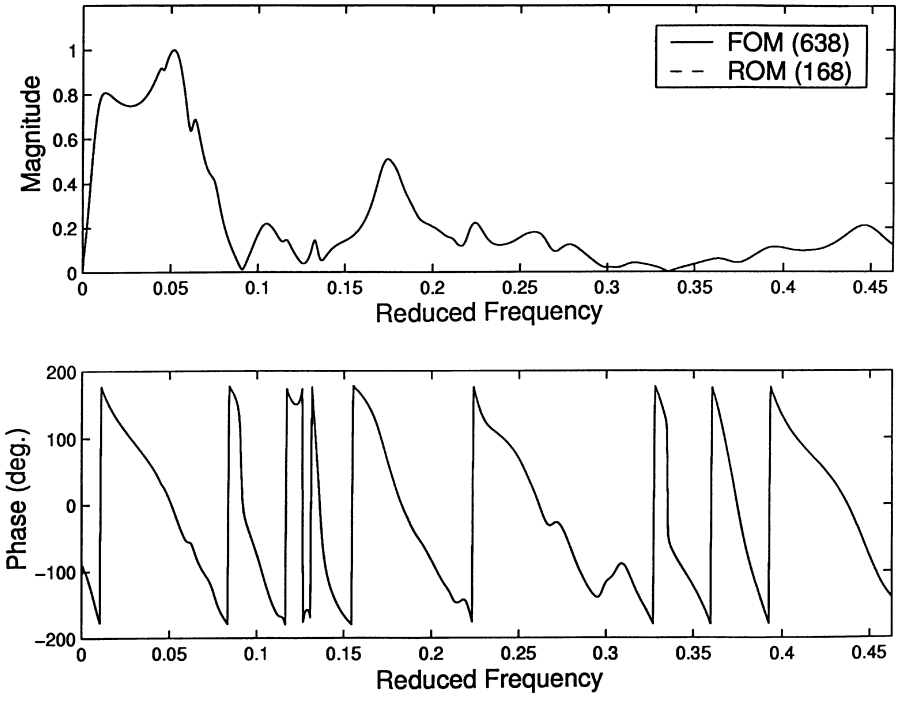

Fig. 3 Wing shear force caused by unit gust (open loop).

domain using the Roger's RFA approximation. The number of lag poles used in the approximation is 4, 8 for the structural modes and gust, respectively. Hence, the size of the state-space aeroelastic matrix $\boldsymbol{A}$ is (638×638). This aeroelastic model contains a few unstable rigid-body modes that are also nearly singular.

Because the aeroelastic matrix $\boldsymbol{A}$ is nearly singular with the few unstable modes very close to the origin, from numerical precision consideration it was necessary to decompose $\boldsymbol{A}$ into its unstable (3×3) and stable (635×635) block-diagonal matrices based on its eigenvalues and eigenvectors and apply the KL procedure only to the latter part of the matrix. The (3×3) submatrix contains one real and one pair of complex eigenvalues that represent, respectively, the airplane phugoid and spiral mode. $\boldsymbol{B}_g$ and $\boldsymbol{B}_\delta$ were also divided into two portions accordingly. The feedback system that generates the elevator command consists of 31 control and 303 measurement states, respectively. Hence, the total number of states in the closed-loop model is 669. The major role of this control system is to alleviate the short-period rigid-body response caused by the vertical gust excitation.

Open-loop state responses of the (635×635) model subjected to independent excitations by the elevator command and vertical gust in the form of a unit impulse were sampled at 16 and 44 reduced frequencies uniformly distributed in (0, 0.00785) and (0.00785, 0.463), respectively. Both responses were sampled to ensure that

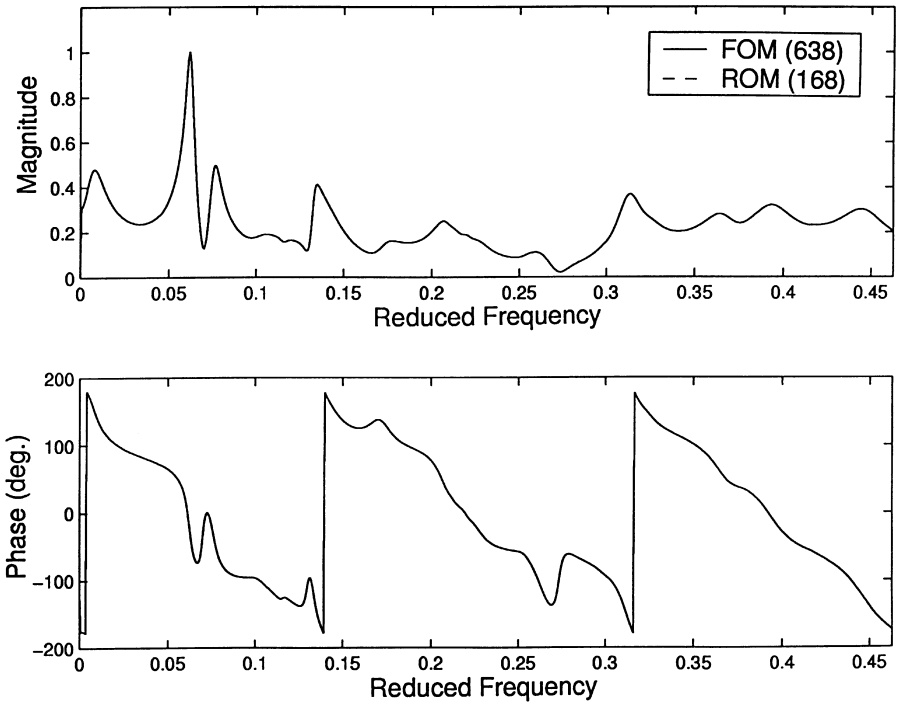

Fig. 4 Pitch rate caused by unit elevator command (open loop).

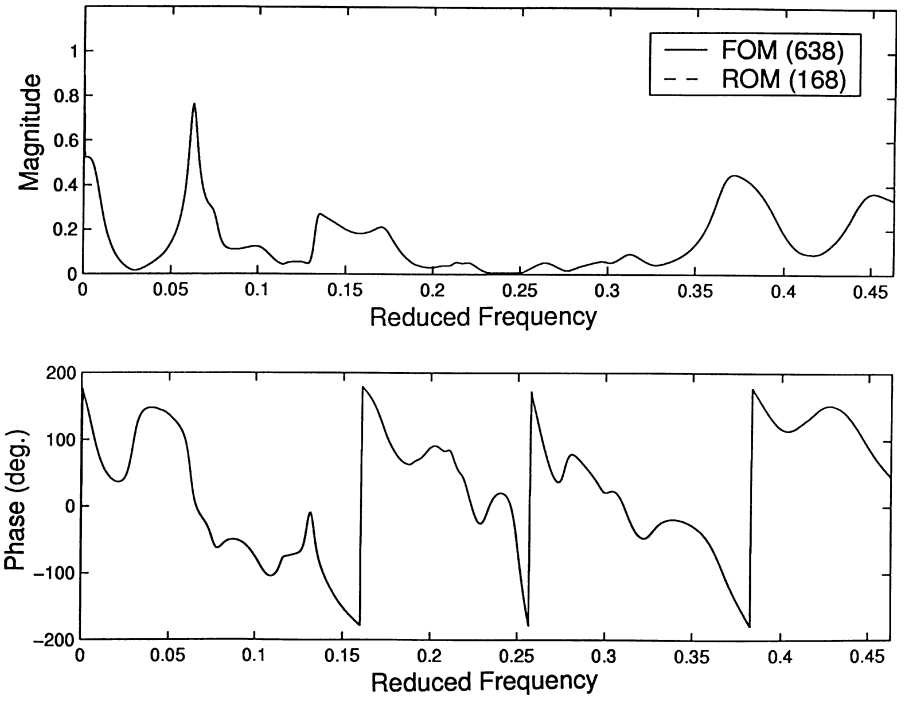

Fig. 5 Wing shear force caused by unit elevator command (open loop).

the final reduced-order model can be used for closed-loop as well as open-loop analyses. Another 120 responses were obtained by taking complex conjugate of these samples. They correspond to the negative frequency range, $(-0.463, 0)$. Thus, a (240×240) snapshot matrix was constructed based on the energy principle, Eq. (24), with equal weights $W_1 = W_2 = 1$, creating a total of 240 optimal modes. After examining the eigenvalues of the snapshot matrix, the first 165 modes that correspond to the largest $\bar{\lambda}_i$ were selected for model reduction. Hence, the size of the resulting reduced-order aeroelastic model became (168×168). These modes were selected conveniently by checking the rank of the snapshot matrix and taking the first rank number of the modes whose KL eigenvalues are in descending order of magnitude.

Figure 1 is eigenspectrum of the reduced-order model (ROM) in the reduced Laplace domain, $\bar{s} = sb/V$. Also presented is the eigenspectrum of the (638×638) full-order model (FOM). It can be seen that most eigenvalues of the reduced system match with eigenvalues of the full model and their imaginary parts are restricted to approximately $(-0.463, 0.463)$, which is the sampling frequency range. Figure 2 is a normalized gust frequency response of pitch rate at one body location as a function of reduced frequency. Figure 3 represents normalized gust responses of vertical shear force at one wing location. Also shown in the plots are the corresponding gust responses from the FOM. There is an excellent agreement between the two sets of the results. In fact, the two sets of the curves are practically identical. Likewise, Figs. 4 and 5 show the same responses as a result of a unit command input for the elevator. Again, the ROM matches with the FOM extremely well in producing these results. The next set of figures, Figs. 6 and 7, are transient responses of the normalized vertical acceleration and wing bending moment caused by an $(1 - \cos)$ discrete gust input. Figures 8 and 9 are transient responses of the same outputs caused by a ramp increase in the elevator control command. Once again, there are excellent agreements between the two models.

Figure 10 shows eigenspectra of the full-order and reduced-order closed-loop matrices. The sizes of these matrices are (669×669)

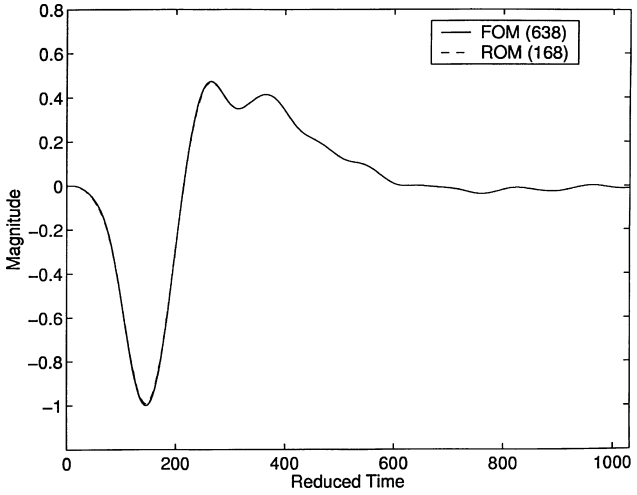

Fig. 6 Vertical acceleration caused by (1 − cos) gust (open loop).

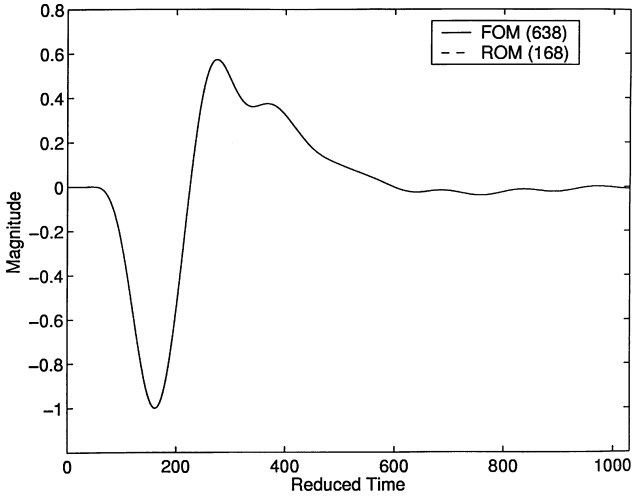

Fig. 7 Wing bending moment caused by (1 − cos) gust (open loop).

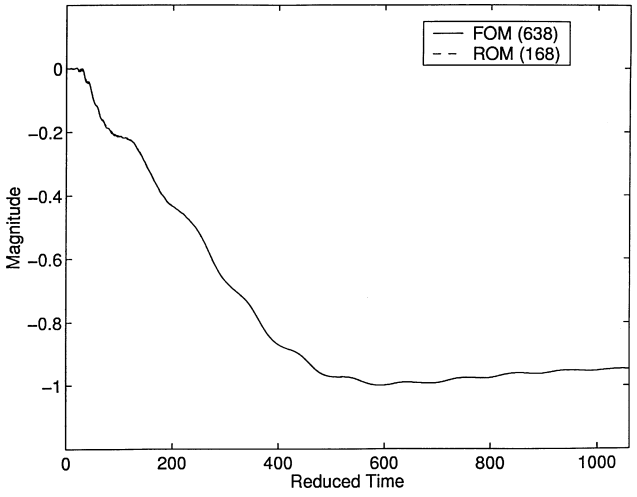

Fig. 8 Vertical acceleration caused by ramp elevator command (open loop).

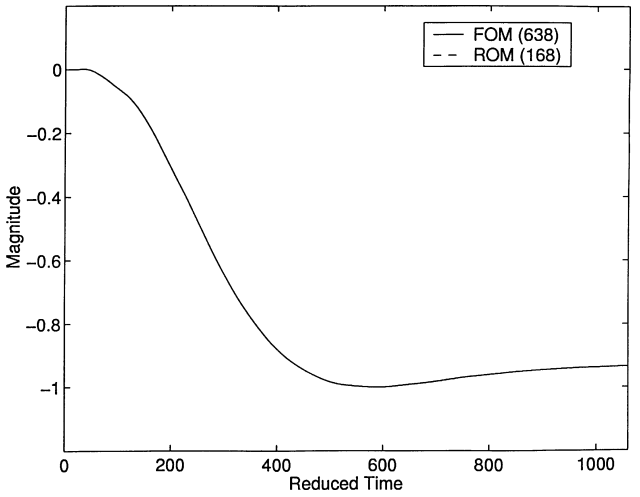

Fig. 9 Wing bending moment caused by ramp elevator command (open loop).

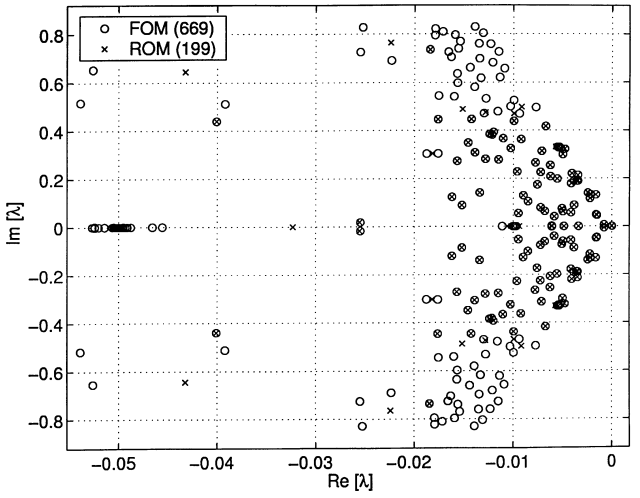

Fig. 10 Aeroelastic root loci of a commercial aircraft (closed loop).

and (199 × 199), respectively. Compared to Fig. 1, the plot contains extra eigenvalues associated with the control law. However, this closed-loop system is still unstable exhibiting three unstable poles. This is because, as stated earlier, the role of the feedback control through the elevator is to attenuate mainly the airplane short-period mode and hence does not significantly alter the unstable modes that exist in the open-loop system. The instability associated with the phugoid mode is caused by lack of longitudinal aerodynamic damping in the analytic model. On the other hand, the instability of the spiral mode can be an intrinsic one, that is, depending on a particular flight condition it could be either unstable or stable. In the next figure, Fig. 11, open-loop and closed-loop pitch-rate responses are compared to illustrate the impact of the feedback control on the airplane performance during the vertical gust excitation. It can be seen that the elevator command input generated by the feedback system clearly attenuates the short-period rigid mode, which is a major contribution to the vertical response while a few elastic modes are amplified by the same control command. Figures 12 and 13 show gust frequency responses of the closed-loop systems that were examined earlier for the open-loop models. Figure 14 represents transient responses of the pitch rate to an (1 − cos) discrete gust input for the closed-loop and open-loop systems. Here, the gust length was adjusted so as to excite mainly the short-period mode. It can be seen that the elevator control does reduce the second peak in the gust response, which represents the transient response to the gust. As in the open-loop cases, all of the results agree well without noticeable differences.

Apart from its high accuracy, the current reduced model is smaller than the size of the p-transform model, which is twice the number of the structural modes. Another advantage is that unlike the

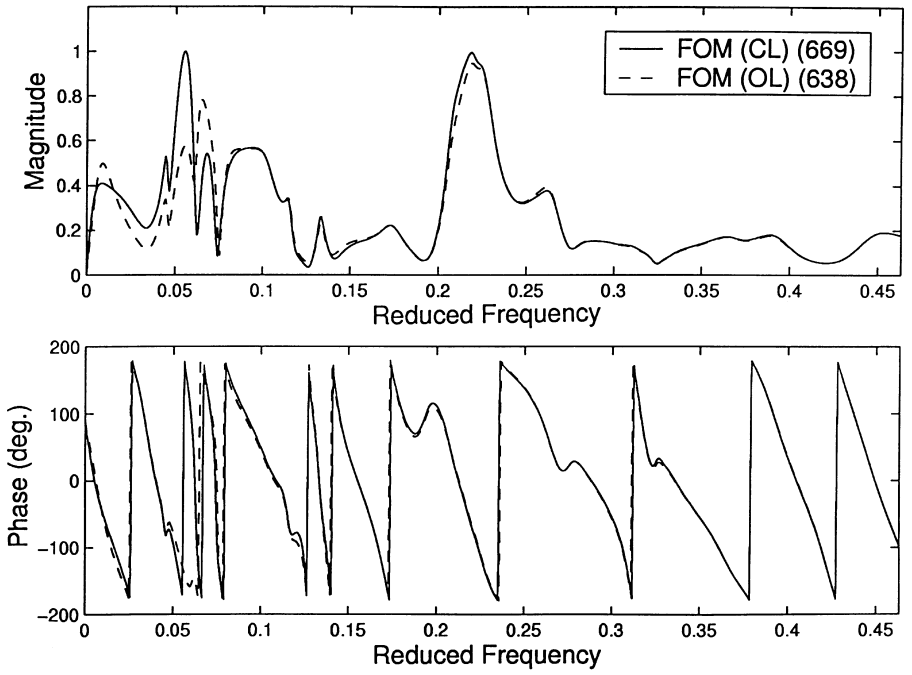

Fig. 11 Pitch rate caused by unit gust (closed loop vs open loop).

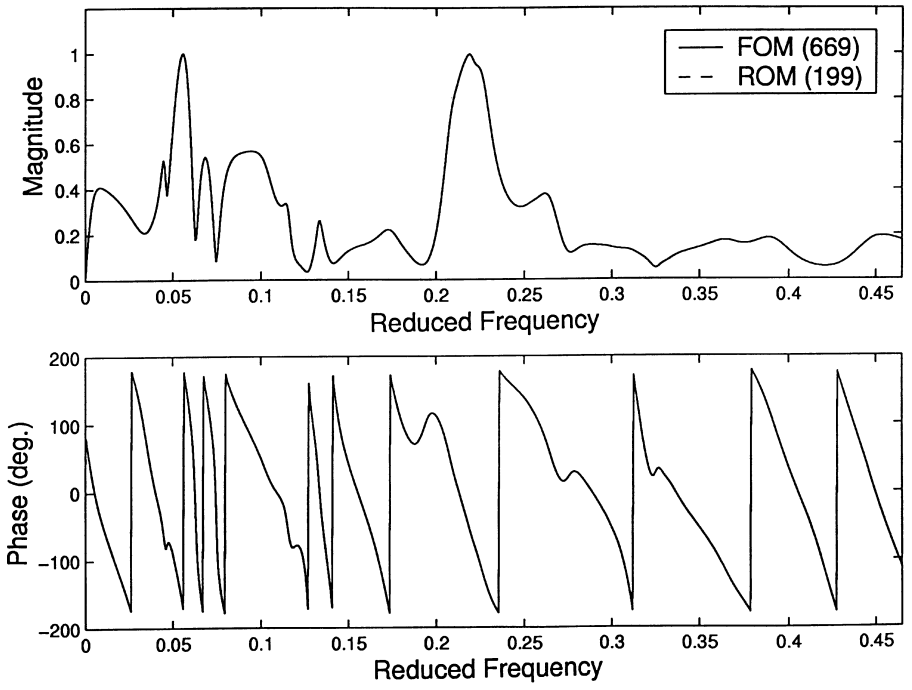

Fig. 12 Pitch rate caused by unit gust (closed loop).

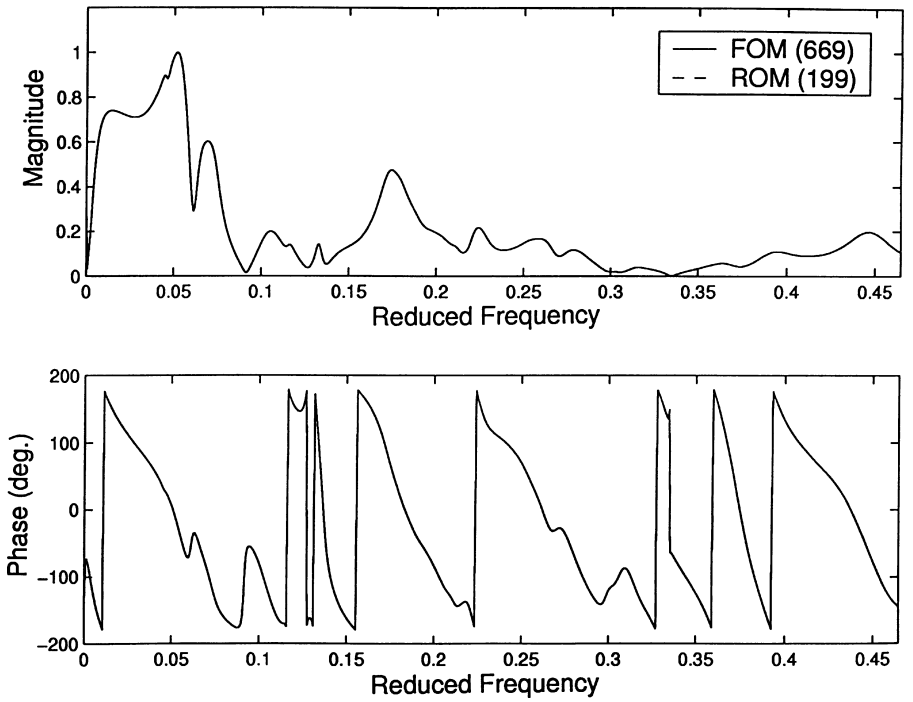

Fig. 13 Wing shear force caused by unit gust (closed loop).

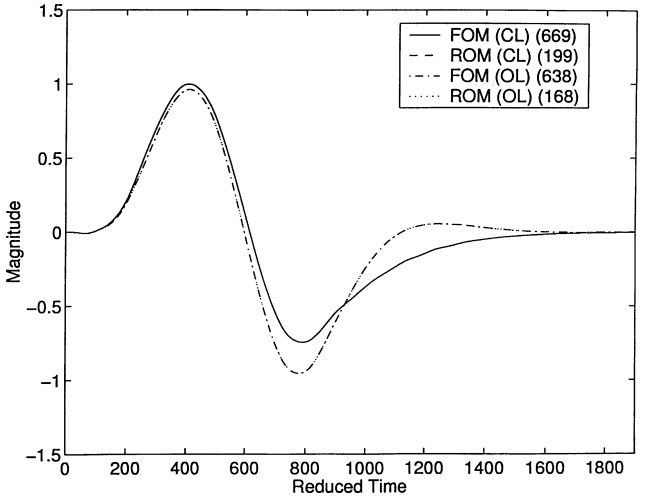

Fig. 14 Pitch rate of the short-period mode caused by (1 − cos) gust.

p-transform model, which is strictly valid only for the open-loop condition for which the k values have been converged, the current open-loop reduced model can be connected to a feedback control to design a closed-loop system. However, if any parameters in the system matrices such as air speed change, the reduction must be performed again for the new parameters, which is also required for the p-transform model. For this reason, the reduced-order model is not recommended for flutter analysis.

Finally, to put a perspective on computational cost associated with the proposed reduced modeling, once the RFA aeroelastic model has been decomposed into the stable and unstable parts for a given flight condition, it takes approximately 180 CPU s on a RS6000 workstation to obtain the optimal modes and perform Galerkin's minimization. After the reduced-order model is constructed, it takes 8 CPU s to create one gust time history response of the open-loop system using 979 time steps, whereas 166 CPU s are required to compute the same response based on the full-order model. Table 1 illustrates the consequence of using the full model vs reduced model for multiple calculations. Clearly, the more the response analysis is executed, the more beneficial it becomes to use the reduced-order

Table 1 Comparison of CPU time for open-loop analysis

Analysis	FOM (638), s	ROM (168), s
Construction	0	180
1st response	166	8
2nd response	166	8
Kth response	166	8
Total	$(K \times 166)$	$(180 + K \times 8)$

aeroelastic model. The present model will be equally useful when designing closed-loop control laws and validating the subsequent closed-loop system. This is because when calculating a control gain based on a numerical algorithm such as the full-state[13] or output feedback[14] the number of equations to solve as well as the amount of memory space required during the process increase approximately proportional to L^2.

Conclusions

In this paper, the Frequency-Domain Karhunen–Loeve method has been applied for model reduction of the Roger's rational function approximation (RFA) aeroelastic model. Using a finite number of open-loop response samples in the frequency domain, optimal modes for the aeroelastic model were calculated, and the general solution was approximated by a linear combination of a few such modes. For demonstration of the method, a representative commercial airplane model with 638 state variables was reduced to a system with only 168 states. For a closed-loop modeling, a feedback system consisting of 31 control, 303 measurement states, and an elevator command input was added to the open-loop model. Based on the study performed on the example model, a number of conclusions can be made as follows. For construction of an open-loop reduced-order model that will later be closed by a feedback system, it is necessary to include both the gust and control command responses in the KL mode calculation. Once constructed, the reduced-order model captures the eigenvalues of the original open-loop and closed-loop systems very accurately. Similarly, the reduced-order aeroelastic model recreates the responses of the full model extremely well both in open-loop and closed-loop analyses. It is interesting that the size of the reduced-order open-loop model could be smaller than the twice the number of structural modes. Considering its size and accuracy,

it can be expected that the reduced model will be very efficient in repeated analysis of dynamic loads, optimization, and closed-loop designs. The procedure is easy to implement, robust, powerful, and can be applied to any type of state-space aeroelastic model.

Acknowledgments

The authors wish to thank William J. Sanders in Dynamic Flight Loads who kindly provided all of the numerical input data for the aeroelastic model studied in this paper.

References

[1]Roger, K. L., "Airplane Math Modeling Methods for Active Control Design," *Structural Aspects of Active Controls*, AGARD-CP-228, Aug. 1977, pp. 4.1–4.11.

[2]Karpel, M., "Design for the Active Flutter Suppression and Gust Alleviation Using State-Space Aeroelastic Modeling," *Journal of Aircraft*, Vol. 19, No. 3, 1982, pp. 221–227.

[3]Karpel, M., and Hoadly, S. T., "Physically Weighted Approximations of Unsteady Aerodynamic Forces Using the Minimum-State Method," NASA TP-3025, 1991.

[4]Mujumdar, P. M., and Balan, N., "Multiple Order Pole Pure Lag Rational Function Approximations for Unsteady Aerodynamics," *Journal of Aircraft*, Vol. 32, No. 2, 1995, pp. 334–342.

[5]Heimbaugh, R. M., "Flight Controls Structural Dynamics IRAD," McDonnell Douglas Rept. MDC-J2303, March 1983.

[6]Winther, B. A., Goggin, P. J., and Dykman, J. R., "Reduced Order Dynamic Aeroelastic Model Development and Integration with Nonlinear Simulation," *Journal of Aircraft*, Vol. 37, No. 5, 2000, pp. 833–839.

[7]Dowell, E. H., Hall, K. C., and Romanowski, M. C., "Eigenmode Analysis in Unsteady Aerodynamics; Reduced-Order Models," *Applied Mechanics Review*, Vol. 50, No. 6, 1997, pp. 371–386.

[8]Kim, T., "Frequency-Domain Karhunen-Loeve Method and Its Application to Linear Dynamic Systems," *AIAA Journal*, Vol. 36, No. 11, 1998, pp. 2117–2123.

[9]Breuer, K. S., and Sirovich, L., "The Use of the Karhunen-Loeve Procedure for the Calculation of Linear Eigenfunctions," *Journal of Computational Physics*, Vol. 96, No. 2, 1991, pp. 277–296.

[10]Winter, M., Barber, T. J., Everson, R. M., and Sirovich, L., "Eigenfunction Analysis of Turbulent Mixing Phenomena," *AIAA Journal*, Vol. 30, No. 7, 1992, pp. 1681–1688.

[11]Kim, T., "An Efficient Response-Based Modal Analysis for Dynamic Systems with Multiple Inputs," AIAA Paper 2001-1380, April 2001.

[12]Nicot, Ph., and Patiau, C., "Aeroelastic Analysis Using Finite Element Models," *Proceedings of the European Forum on Aeroelasticity and Structural Dynamics*, Aachen, Germany, April 1989.

[13]Maciejowski, J. M., *Multivariable Feedback Design*, Addison Wesley, Longman, Reading, MA, 1989, Chap. 5.

[14]Athans, M., and Levine, W. S., "On the Determination of the Optimal Constant Output Feedback Gains for Linear Multivariable Systems," *IEEE Transactions on Automatic Control*, Vol. 15, No. 1, 1970, pp. 44–48.